Proceedings of the 17th International Symposium on the Packaging and Transportation of Radioactive Materials
PATRAM 2013
August 18-23, 2013, San Francisco, CA, USA

Reversal Bending Fatigue Test System for Investigating Vibration Integrity of Spent Nuclear Fuel during Transportation*

J-A. Wang, H. Wang, B. B. Bevard, R. L. Howard
Oak Ridge National Laboratory

M. E. Flanagan
U.S. Nuclear Regulatory Commission

ABSTRACT

Transportation packages for spent nuclear fuel (SNF) must meet safety requirements under normal and accident conditions as specified by federal regulations. During transportation, SNF experiences unique conditions and challenges to cladding integrity due to the vibrational and impact loading during road or rail shipment. Oak Ridge National Laboratory (ORNL) has been developing testing capabilities that can be used to improve the understanding of the impacts on SNF integrity due to vibration loading, especially for high burn-up SNF in normal transportation operation conditions. This information can be used to meet the nuclear industry and U.S. Nuclear Regulatory Commission needs in the area of safety and security of spent nuclear fuel storage and transportation operations.

The ORNL developed test system can perform reversal-bending fatigue testing to evaluate both the static and dynamic mechanical response of SNF rods under simulated loads. The testing apparatus is also designed to meet the challenges of hot-cell operation, including remote installation and detachment of the SNF test specimen, in-situ test specimen deformation measurement, and implementation of a driving system suitable for use in a hot cell. The system contains a U-frame set-up equipped with uniquely designed grip rigs to protect the SNF rod sample and to ensure valid test results, and uses 3 specially designed LVDTs to obtain the in-situ curvature measurement.

A variety of surrogate test rods have been used to develop and calibrate the test system as well as in performing a series of systematic cyclic fatigue tests. The surrogate rods include stainless steel (SS) cladding, SS cladding with cast epoxy, and SS cladding with alumina pellet inserts simulating fuel pellets. Testing to date has shown that the interface bonding between the SS cladding and the alumina pellets has a significant impact on the bending response of the test rods as well as their fatigue strength. The failure behaviors observed from tested surrogate rods provides a fundamental understanding of the underlying failure mechanisms of the SNF surrogate rod under vibration which has not been achieved previously. The newly developed device is scheduled to be installed in the hot-cell in summer 2013 to test high burnup SNF.

I. INTRODUCTION

Spent fuel transportation has long been established as an important part of the industrial activities in the backend of the nuclear fuel cycle. An important factor to be taken into account is the current trend toward higher burnup, driven mainly by economic incentives in the competitive power market. Transportation packages for spent nuclear fuel (SNF) must meet safety requirements specified by federal regulations. For normal conditions of transport, vibration loads incident to transport must be considered. This is particularly relevant for high-burnup fuel (>45 GWd/MTU). As the burnup of the fuel increases, a number of changes occur that may affect the performance of the fuel and cladding in storage and during transportation. Spent fuel cladding has traditionally provided defense-in-depth as the primary fission product barrier in the nuclear fuel cycle, and has been relied upon to provide geometry control for criticality safety during transportation. The mechanical properties of high-burnup de-fueled cladding have been previously studied by subjecting defueled cladding tubes to longitudinal (axial) tensile tests, ring-stretch tests, ring-compression tests, and biaxial tube burst tests. The objective of this study is to investigate the mechanical properties and behavior of both the cladding and the fuel in the cladding (including inertia induced fuel pellet and clad interaction) under vibration/cyclic loads similar to the sustained vibration loads experienced during normal transport.

The vibration loads experienced by SNF rods during transportation can be characterized by dynamic, cyclic, bending loads. The transient vibration signals in a specified transport environment can be analyzed, and frequency, amplitude and phase components of the vibration can be identified. The methodology being developed at Oak Ridge National Laboratory (ORNL) is a novel approach to support the study of the vibration integrity of actual SNF rod segments through the testing and evaluation of the fatigue performance of SNF rods at defined frequencies and loads. ORNL has developed a reversal pure bending fatigue system to evaluate the response of the SNF rods to vibration loads as noted in Refs 1, 2 and 3. A three-point deflection measurement technique using linear variable differential transformers (LVDTs) is used to characterize the rod curvature of samples under test conditions, and electromagnetic force linear motors are used as the driving system to provide the mechanical load. ORNL plans to use the test system in a hot cell to perform SNF vibration testing on high burnup fuel to evaluate the effect of pellet-clad interaction and effects of material bonding on the effective lifetime of the fuel-clad structure bending fatigue performance. A brief introduction of this test system will be provided in this paper along with some preliminary test results.

II. TEST SYSTEM CONCEPT

The reversal pure bending is conducted using a U-frame testing setup. A vertical U-frame setup is shown in Fig. 1. The U-frame is constructed with two rigid arms and the associated linking members. The rod specimen is coupled with the U-frame by inserting it into the co-linear holes within the two rigid arms. As a result, reversal bending will be applied to the rod specimen when a controlled push-pull force is applied to the two loading points of the rigid arms. To control any contact-induced damage to the rod specimen, compliant layers are used between the test rod and the rigid arm. This proposed test system is able to capture the pure reversal bending as desired and at the same time, is easy to use and compliant with all requirements of the hot cell test facility. The system has a minimal number of moving parts, and test sample installation can be achieved using a simple drop-in action. The

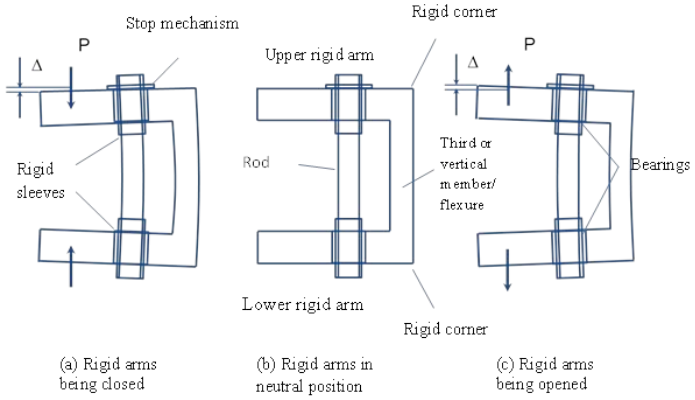

Fig. 1. U-frame-assisted bending fatigue testing setup for reversal bending when rigid arms are (a) closing, (b) neutral, and (c) opening.

test system is designed to use a 6-inch rod segment with 2-inch gage section. Initial test specimens will come from high burnup SNF rods with Zircaloy-4 cladding. The majority of the test system components are made of stainless steel (SS) 304. Prior to initial equipment design, 3-D finite element analysis (FEA) showed that the position of the rod specimen relative to the linking member of the U-frame has a significant impact on the amount of stress applied to the specimen. Using appropriate compliant layers allows a pure bending moment to be achieved in the gage section as shown in Fig. 2. The maximum von Mises stress level occurs at the pellet-clad interface.

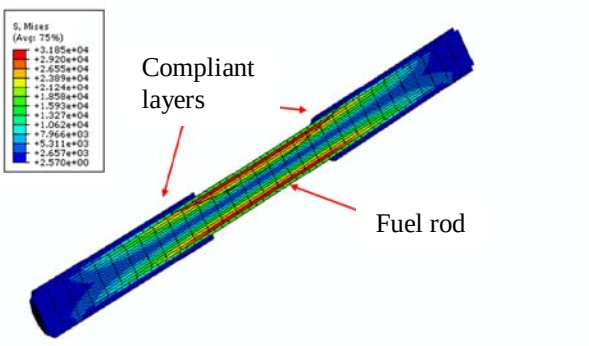

Fig. 2 Stress distribution in a fuel rod with compliant layer when the applied force was 178 N; the unit of stress is psi. The maximum von Mises stress is 220 MPa (3.185×104 psi).

III. DEVELOPMENT OF TEST SYSTEM

The first generation (1G) of the test setup was fabricated and assembled on an MTS servo-hydraulic test machine, shown in Fig. 3. It was discovered that the use of a PTFE (Teflon) compliant layer required a press-fit process for installation on the rod specimen, and the press-fit installation apparently offsets the advantage of the U-frame setup of easy installation of the test sample.

A fundamental change was made to the test setup to introduce linear ball bearings (LBB) into the rigid arms. Using LBB, the test specimen can be "dropped-in" the U-frame; that significantly reduces the effort to install the test specimen. Also, it was found that the specimen needed to be prepared for installation into the U-Frame with pre-machined rigid sleeves already assembled onto the rod specimen using a dedicated procedure. A more advanced modification developed for the 3G setup involved the use of pre-loaded linear roller bearing (LRB) sets embedded in the rigid arms along with the hexagonal rigid sleeves for the test specimen. The introduction of LRB removed the backlash experienced during reverse bending in previous designs, while at the same time, maintained the feature of using the test specimen dropping-in design. A 3G U-frame setup is shown in Fig. 4.

An additional difference between the 1G and 3G setup (Fig. 3 and Fig. 4) is the addition of counterweights on the side of the rigid arms opposite the rod specimen in the 3G design. The

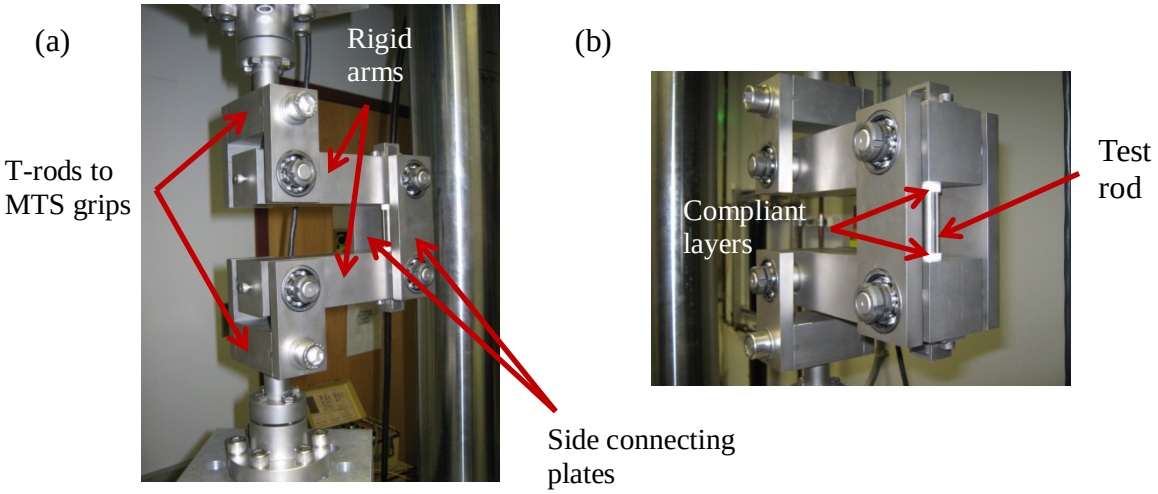

Fig. 3. (a) Assembled U-frame setup on MTS testing machine (809), and (b) end view illustrating the rod under test. Loading arm is 152.4 mm. Teflon is used as compliant layers, and the rod is press-fit into the specimen holes of the two rigid arms.

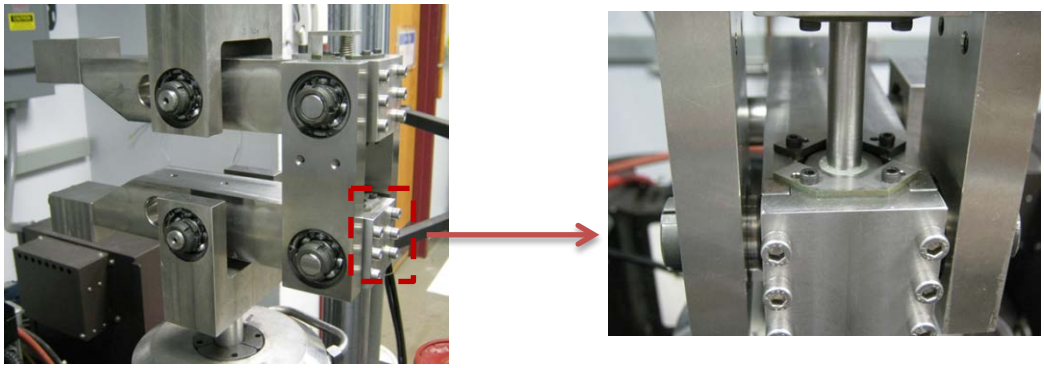

(a) (b)

Fig. 4. (a) 3G U-frame setup equipped with linear roller bearings (LRBs) that are preloaded by bolt-tightening the end blocks. The enlarged view in (b) shows the rod inserted.

counterweights mitigate the effect of the self-weight of the U-frame components due to gravity, and ensure that the stress state of the rod specimen is pure bending as designed. Upon further testing, it was noted that the use of counterweights could potentially limit the usable frequency range of the system or limit the dynamic displacement because the system would have to consume a substantial amount of input energy to overcome the inertia and damping effect.

A new generation of U-frame has been developed that has the U-frame set horizontally, and uses a dual Bose linear motor TestBench (Fig. 5). This alignment eliminates the effect of the U-frame self-weight entirely; also the push-pull force is applied symmetrically at both loading points by use of the dual motors. This design allows the use of a wide frequency range when applying pure bending to the test specimen during dynamic cycling. Moreover, the Bose linear motors use electromagnetic forces to generate the driving forces and thus there are no oil issues as would occur when using a servo-hydraulic test machine.

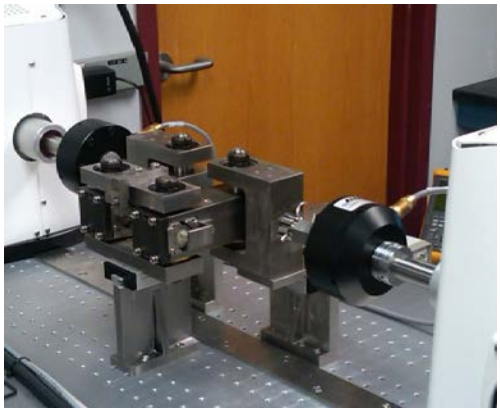

Fig. 5. Integrated ORNLU-frame Bose dual linear motor TestBench. A horizontal arrangement is used to eliminate the effect of the U-frame mass on the specimen.

IV. DEVELOPMENT OF MEASUREMENT METHODS

In a hot cell or out-of-cell environment, LVDTs are one of the most reliable methods available for measuring the deformation of a rod specimen during bend testing. Even when using this measurement method, there is still a significant challenge to collecting accurate bending data because both the deformation of the compliant layers and the rigid body motion of the test frame contribute to the measured results. A three-point measurement system has been implemented to accurately capture the deformation of the rod specimen during testing. The three-point measurement system involves using three LVDTs spaced along the test specimen to accurately measure the deflection over a wide area of the specimen. The three LVDTs are assembled into a single sensor clamp and are mounted to the side connecting plates. The total curvature of specimen can be deduced from the LVDT measurements and this information can be used to characterize the true deformation of the specimen. The deformation information collected using this measurement system is relatively independent of the compliant layers and rigid body motion of the U-frame system. The three-point measurement method is shown in Fig. 6.

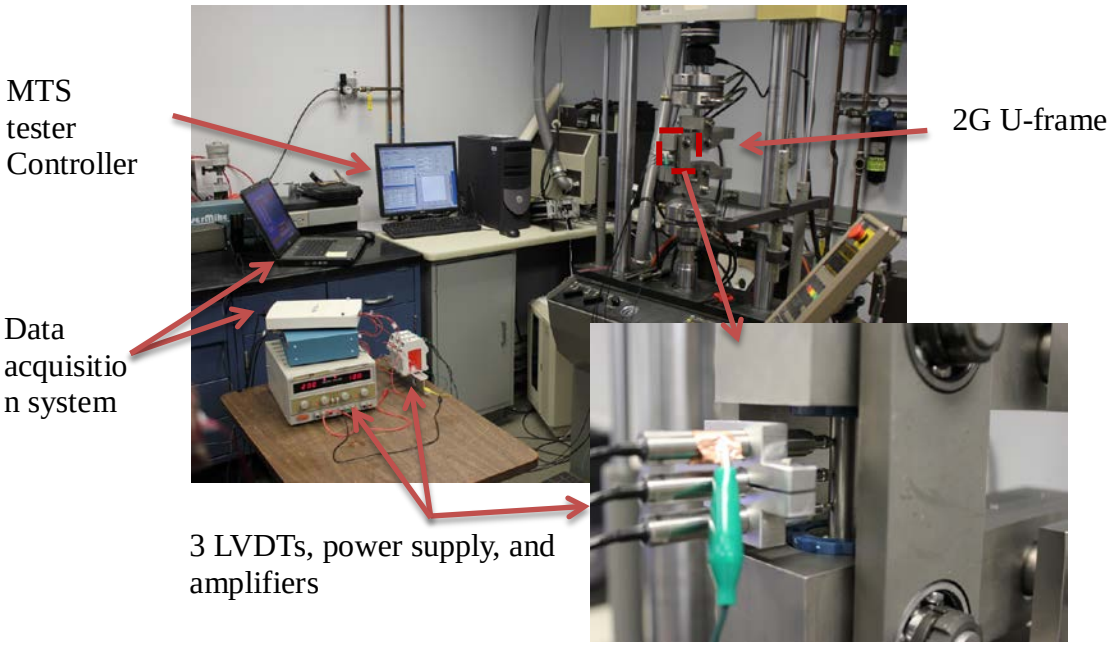

Fig. 6. Three-point measurement method for the curvature of specimen through three LVDTs. The demonstration is on the U-frame setup equipped with linear ball bearings and integrated onto a MTS 810 servo-hydraulic test machine.

The use of curvature along with the bending moment enables the rod specimen to be tested and characterized more appropriately than using a single point deflection measurement, substantially reducing the uncertainty. The curvature obtained using a surrogate rod made of SS tube is given in Fig. 7. It can be clearly seen that in a force control mode, the waveform of curvature followed that of the moment.

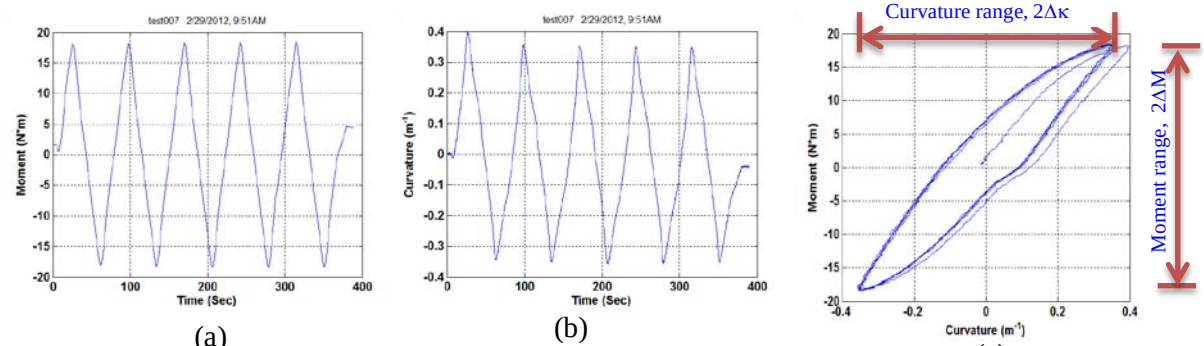

(a) (b) (c)

Fig. 7. (a) Moment curve, (b) curvature curve, and (c) moment–curvature loops obtained by use of 3G U-frame with preloaded LRBs. The results are based on the rod made of SS tube only using the LRB U-frame on MTS 810 test machine under ±180 N, 10 N/s.

The moment-curvature relationship revealed a significant amount of hysteresis because of plastic deformation. However, the amplitude response will be focused as follows: the flexural rigidity is defined as a ratio of moment range, ΔM to curvature range; Δκ will be used to characterize the property of the rod specimen,

Flexural Rigidity, $EI = \Delta M/\Delta\kappa$. (1)

It is seen that in an elastic system, the flexural rigidity is determined by $E*I$ in which E is Young's modulus and I is the moment of inertia. The flexural rigidity should characterize the bending stiffness in some sense, while the latter also depends on the gage length. It is noted here that for a SNF rod, if one assumed perfect bonding between fuel and clad the system flexural rigidity (EI) can be written as,

$$EI_{System} = E_{Fuel}\, I_{Fuel} + E_{Clad}\, I_{Clad}$$

However, if the cohesion bonding at the pellet-clad interface was not good or compromised due to vibration loading, the SNF system EI can be written as

$$EI_{System} = E_{Fuel}\, I_{Fuel} + E_{Clad}\, I_{Clad} - f\,(loading,\ frequency,\ temperature,,)$$

Where, function f is the correction factor to take into account the interface cohesion bond evolution, and is function of vibration loading, frequencies, and temperature as well as clad-pellet interaction mechanism. As shown in Fig. 7 (c), the hysteresis (loop area) is another important physical quantity revealed from the reversal bending vibration testing, which will be studied in the future.

The flexural rigidity of testing rod depends on both rod structure and curvature (load) level as shown in Fig. 8. This characteristic was illustrated from a series of testing on the surrogated rods, made of SS tube, SS tube with alumina pellet (no epoxy bond, which resemble fresh fuel pellet inserts), and SS tube filled with epoxy. The moment-curvature relation is strongly related to rod structure as shown in Fig. 8 (a), while as system flexural rigidity of tested rods, shown in Fig. 8 (b), is dependent on both rod structure and curvature level. The epoxy has significant lower stiffness compared to alumina, however, it provides continuous support and has strong bonding to the SS tube, this in turn provides a higher system stiffness (EI) compared to that of the SS tube with alumina insert only; while as for SS tube with pellet inserts, the pellet insert will start to carry more load when the clad reaches certain curvature levels. SS tube w/o internal support from alumina insert or filled epoxy has the lowest flexural rigidity.

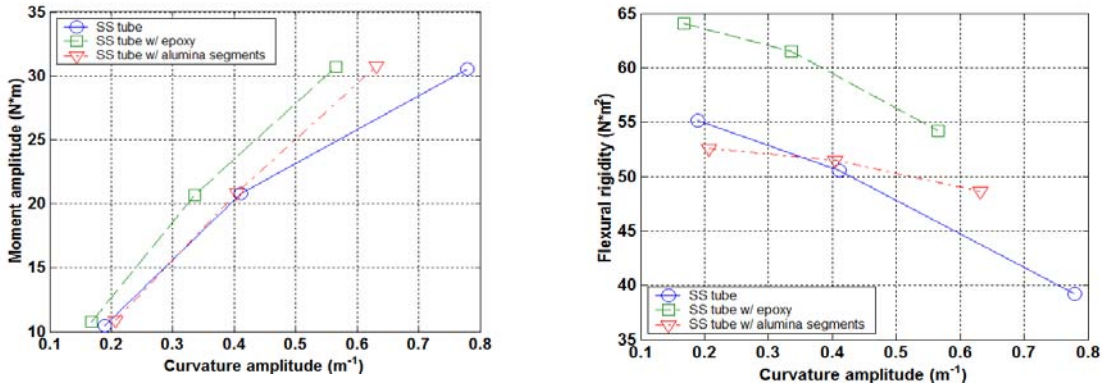

(a) (b)

Fig. 8 Moment-curvature response and the associated system rigidity evaluation.

V. TEST PROTOCOL AND EXPERIMENTAL DEMONSTRATION

A test protocol has been proposed as shown in Fig. 9 for the reversal pure bending fatigue test. The protocol mainly consists of the measurement under quasi-static cyclic loading at the specified number of cycles and the cycling itself. The latter is the dynamic cyclic test at a defined frequency and amplitude.

Surrogate rods have been used extensively in the out-of-cell U-bent integrated fatigue bending tester development. Two series of surrogate rods were made using SS cladding and alumina pellets. One series had the alumina pellets press-fit into the SS cladding and the second series had the alumina pellets bonded both to themselves and to the SS cladding using cast epoxy, expressed with prefixed SSAP.

Initial tests were conducted on a MTS 810 servo-hydraulic machine in displacement control mode using the 3G U-frame test setup. Results for one of the tests, SSAP05, with bonded pellets are shown in Fig. 10. The curvature of this test was fairly flat. The measurement process obviously captured the fracture of the rod specimen indicated by the sudden drop in monitored moment. The flexural rigidity dropped due to cyclic fatigue, with a 16% decrease in rigidity prior to failure. This shows that the flexural rigidity can serve as an index of the structural integrity of rod specimens. Fig. 11 shows curvature and hysteresis loop responses under cyclic bending for the SSAP06 sample under different loading amplitudes applied at U-bent rigid arms. SSAP06 test result shows that the increased curvature and the decreased flexural rigidity are due to cyclic loading.

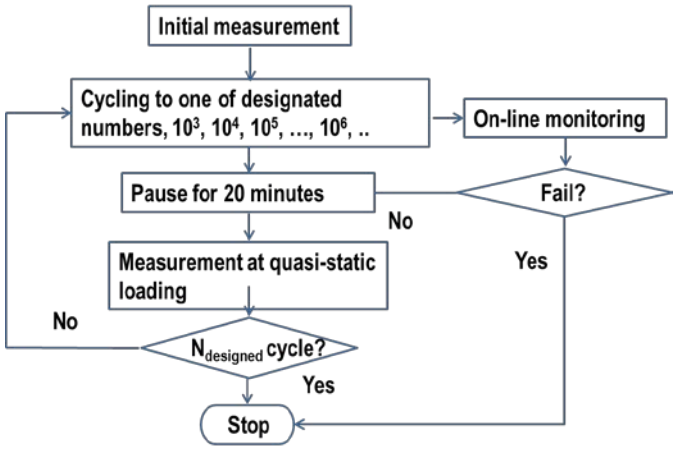

Fig. 9 Test protocol for reversal bending test.

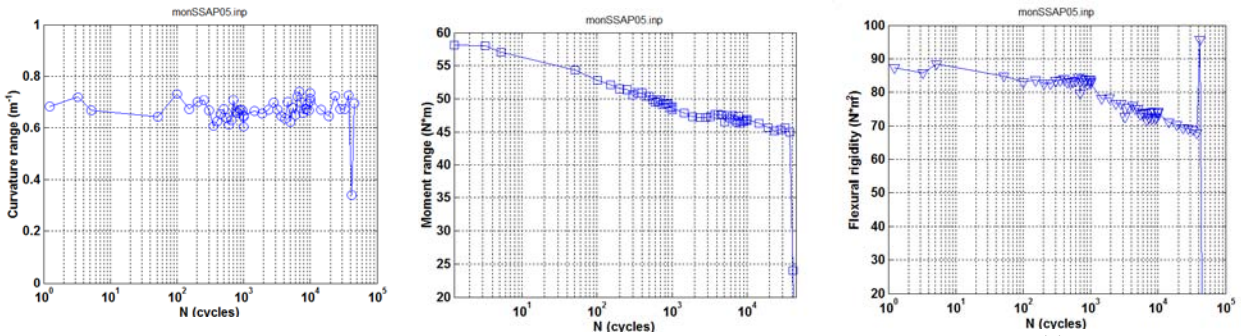

(a) (b) (c)

Fig. 10. Variation of (a) curvature, (b) moment, and (c) rigidity based on on-line monitoring of SSAP05: ±3 mm, 2 Hz. Specimen with octagonal rigid sleeve without Teflon sheets attached; $N_f = 3.7\times10^4$ cycles.

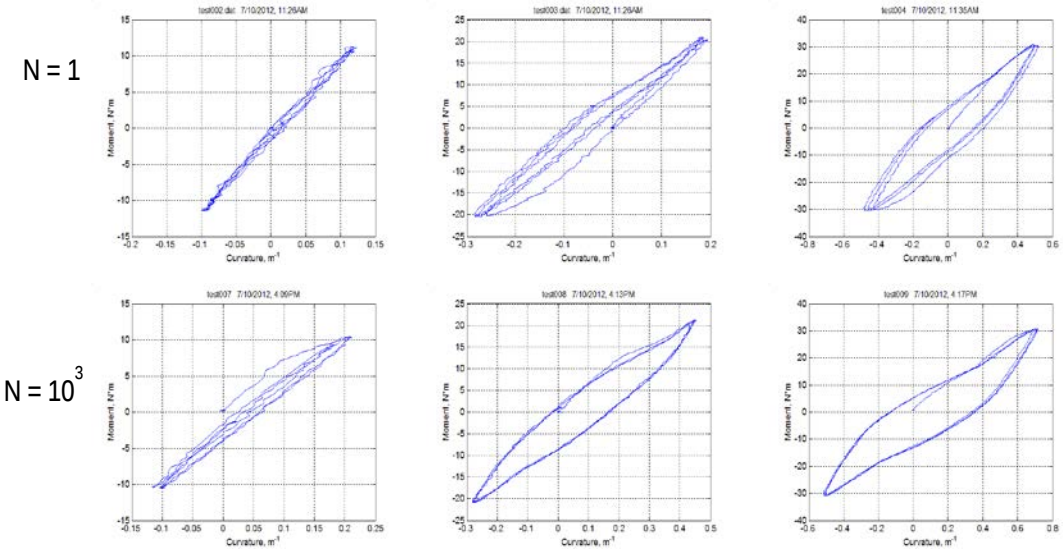

Load amplitude: 100N 200N 300N

Fig. 11 Cycling loading results in increases in curvature and hysteresis; measurements were conducted under load control mode on SSAP06 sample.

Other examples of property changes during the cyclic bending loading from flexural rigidity curves is illustrted in Fig. 12. Fig. 12(a) shows decreased flexural rigidity under increased load and under increased loading cycles from SSAP02 sample, at interval of 1, 1000 and 10000 cycles. It's noted here that SSAP02 has alumna pellet inserts but w/o epoxy bond. The decreased flexural rigidity with increase load level can be referred to test rod nolinear response (or yield) under increased loading. Significant decrease in flexural rigidity of SSAP02 could be the reault of direct pining effect of alumina pellet to the clad and resulting in localized yielding at the clad tube. Fig. 12(b) shows opposite trends under increased curvature, and reveal similar trends of flexural rigidity decrease under increased loading cycles. Due to the linear response of moment-curvature responses, no crack growth in SSAP system will be expected, the decreased flexural rigidity related to cycle frequency of SSAP04 is likely associated with the progressive degradation of the interface bonding between pellet-pellet and pellet-SS tube.

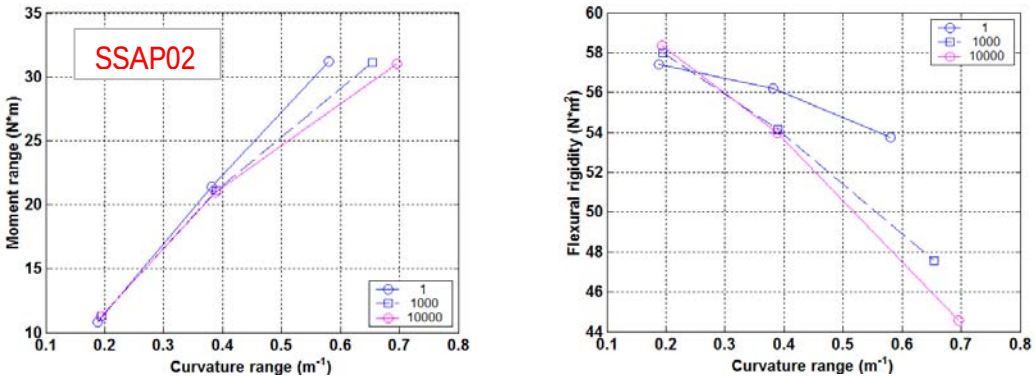

Fig. 12(a) Flexural rigidity property change results from cyclic loading. The measurements were conducted under static cyclic loading at specified points of cycle test.

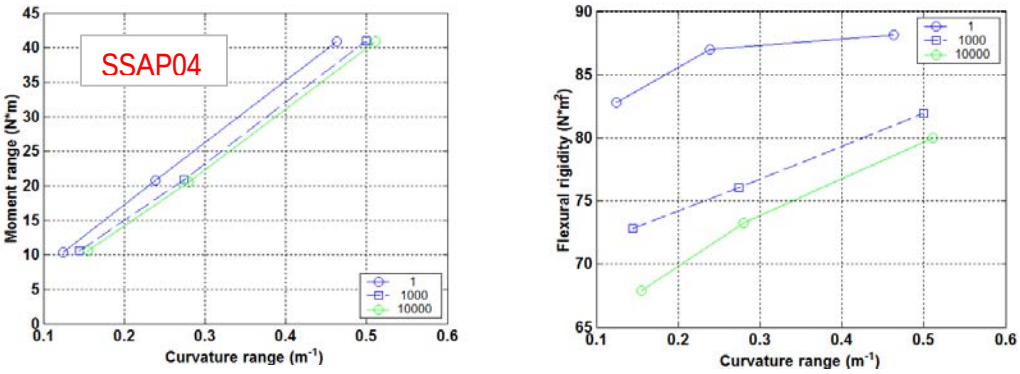

Fig. 12(b) Moment-curvature curves appeared to be quite linear in the tested range for SSAP04. Higher flexural rigidity was observed compared to SSAP02 due to epoxy bond of SSAP04. More significant decrease was observed in rigidity at higher cycles.

VI. OUT-OFF-CELL PROOF OF METHODOLOGY TEST PLAN

The proof of principle demonstrations were performed on the integrated Bose U-bent tester under the load control mode. The main purpose of the proof-of-the principle testing is to demonstrate the repeatability and reliability of the developed reversal U-bent tester in applying to SNF vibration integrity investigation. The surrogate rods made of SS tube embedded with epoxied alumina pellets (SSAP samples) were used for demonstration testing. The tensile test results of the SS tube, based on ASTM E8 tubular testing, is shown in Fig. 13, and the estimated mechanical properties are: E = 176 GPa, YS at 0.2% offset = 325 MPa, UTS = 664 MPa.

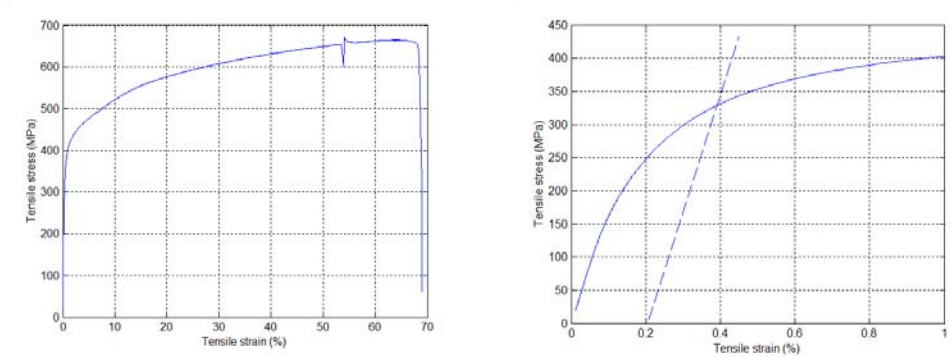

Fig. 13 Axial tensile test results for stainless steel tubing used as surrogate rod for bending testing.

The reversal U-bent apparatus was integrated into a dual motor Bose system and served as the driver to conduct both the static and dynamic fatigue bending tests. The integrated testing device is shown in Fig. 14, where the Bose linear motors are shown to the left, the curvature measurement device of 3-LVDTs is shown to the right of Fig. 14.

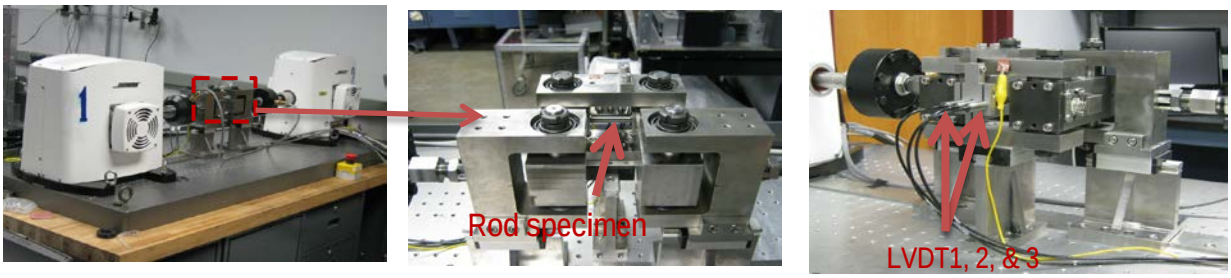

Fig. 14 Integrated Bose reversal U-bent tester used for static and dynamic fatigue bending testing.

Three static bending tests were conducted with a maximum displacement amplitude of 20-mm at the loading point, and the static bending test results are shown in Fig. 15. Based on these test data, the three targeted dynamic bending loading levels were selected, namely, 20 N-m, 25 N-m, and 30 N-m ranges. Based on these moment loading ranges, a series of reversal bending fatigue tests were conducted. The summary of fatigue test results are shown in Fig. 16, and showed that the general trend of fatigue strength is consistent with that of typical S-N trend curve. In order to validate the reliability of epoxy compliance materials, two of the SSAP samples were exposed to spent fuels; the test results show that the compliance material was intact and the fatigue data are consistent with these of non-irradiated SSAP samples.

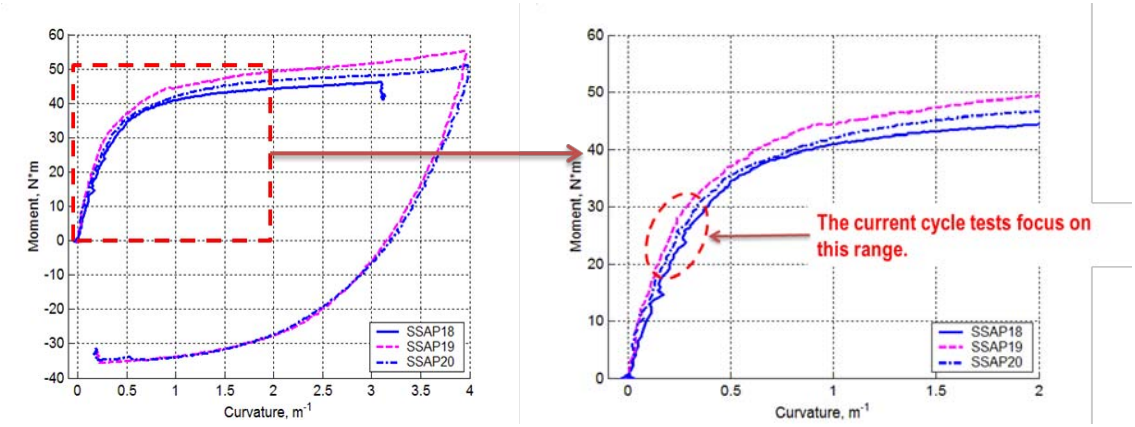

Fig. 15 Static bending test result reveals good repeatability of developed testing protocol.

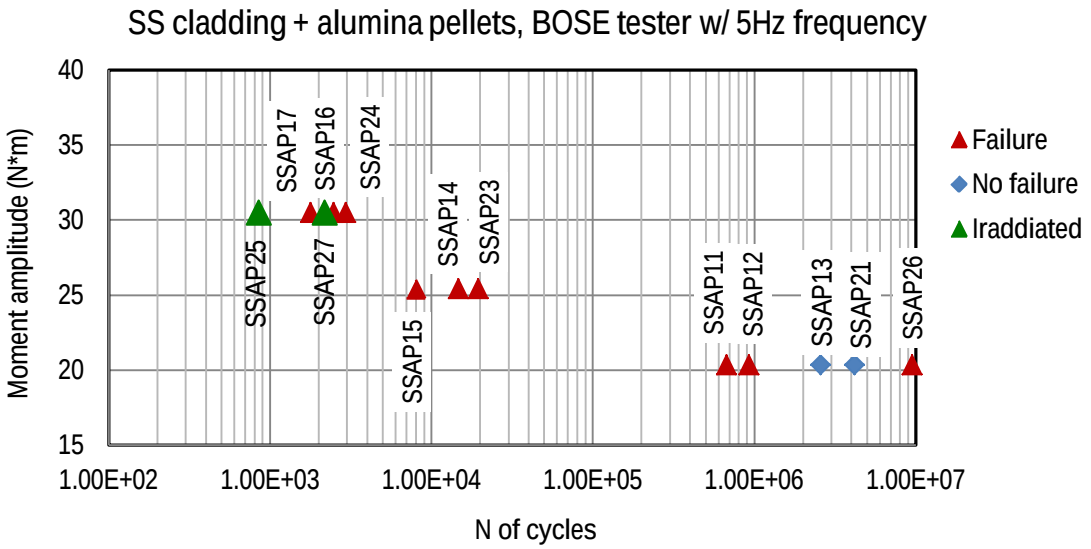

Fig. 16 Reversal bending fatigue tests of SSAP samples show typical S-N trend; cycles of SSAP26 include 5.4M at 10Hz testing; SSAP25 was irradiated 2 weeks between 6- and 7-fuel rod layers and SSAP27 was irradiated in the same fuel pile for 4 weeks.

The above mentioned proof-of-principle testing successfully demonstrated the following:

(1) Repeatability of static testing results for a SSAP material,
(2) Static testing data can be used to set meaningful test conditions for dynamic testing,
(3) Repeatability of dynamic testing results for SSAP material,
(4) The trend for dynamic testing at three different levels produced the expected S-N curve behavior,
(5) Exposing the epoxy in the compliant layer to an irradiation environment revealed no deleterious effects of irradiation on the epoxy.

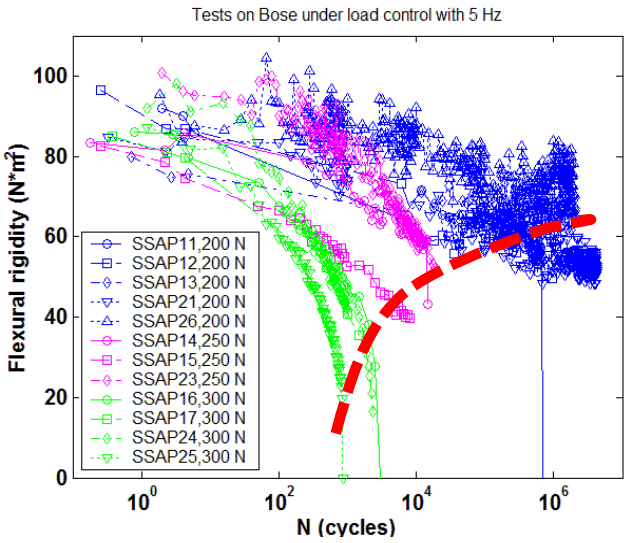

Fig. 17 The evolution of SSAP flexural rigidities under different reversal bending fatigue loadings.

A summary plot of real-time flexural rigidity evolution for tested SSAP samples fracture on the Bose machine is shown in Fig. 17. There are five repetitions at 200 N, three repetitions at 250 N and four repetitions at 300 N loading levels; and there is more variability for the tests at 200N loading level. A red dash line indicated in Fig. 17 is used to connect the residual flexural rigidity strength upon final fracture of SSAP samples. Such a trend curve can be useful in developing governing equations to predict the lifetime of SNF rods under vibration induced accumulated fatigue damage.

All the fractured SSAP samples failed at the gage section as designed, some of the fractured samples and the associated flexural rigidity evolution are shown in Fig. 18 and Fig. 19 for SSAP 11 and SSAP 12 samples, respectively.

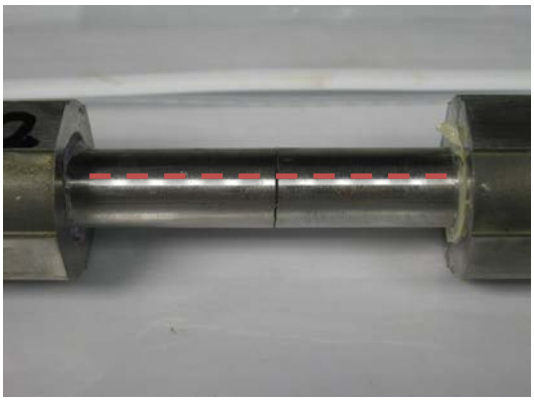

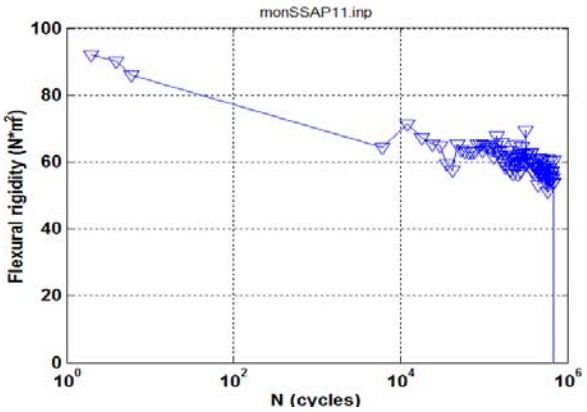

Fig. 18 Test for SSAP11 was conducted on Bose with original setup: load ±200 N, moment ±20.38 N*m, 5 Hz. Initial displacement ±2.5 mm, initial curvature ±0.27 /m, initial strain ±0.14%. Specimen fractured near 678K cycles. About 40% drop in flexural rigidity occurred.

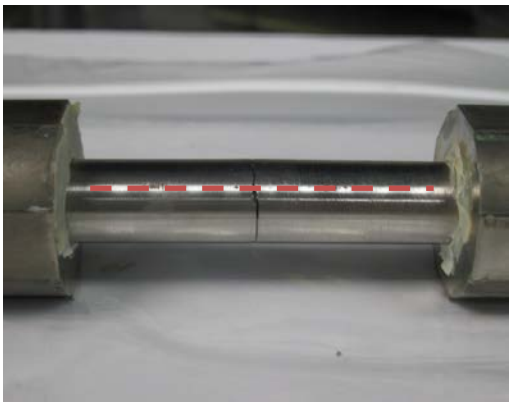

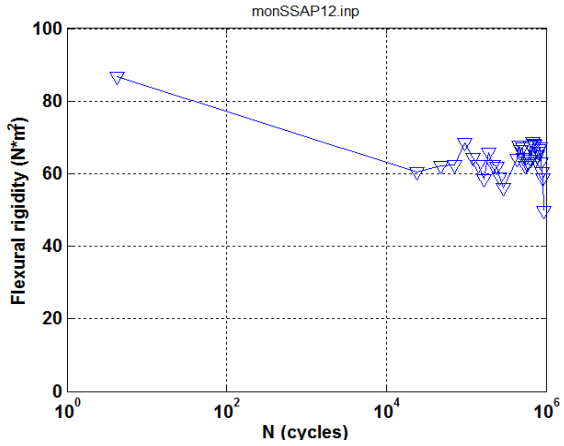

Fig. 19 Test for SSAP12 was conducted on Bose with modified setup under condition: load ±200 N, moment ±20.38 N*m, 5 Hz. Initial displacement ±2 mm, initial curvature ±0.23/m, initial strain ±0.13%. Specimen fractured near 936K cycles. About 42% drop in flexural rigidity.

VII. LOAD CONTROL VS DISPLACEMENT CONTROL BENDING DATA

The reversal bending fatigue tests under displacement control were conducted on the MTS machine with a maximum of 2 Hz cyclic loading frequency. The real-time moment and curvature data comparison between the Bose (load control test) and MTS (displacement control test) tester are shown in Fig. 20. The load control protocol is immune to the impact of the system compliance to the moment value, and appears to be more robust for hot-cell application and further fatigue data analysis.

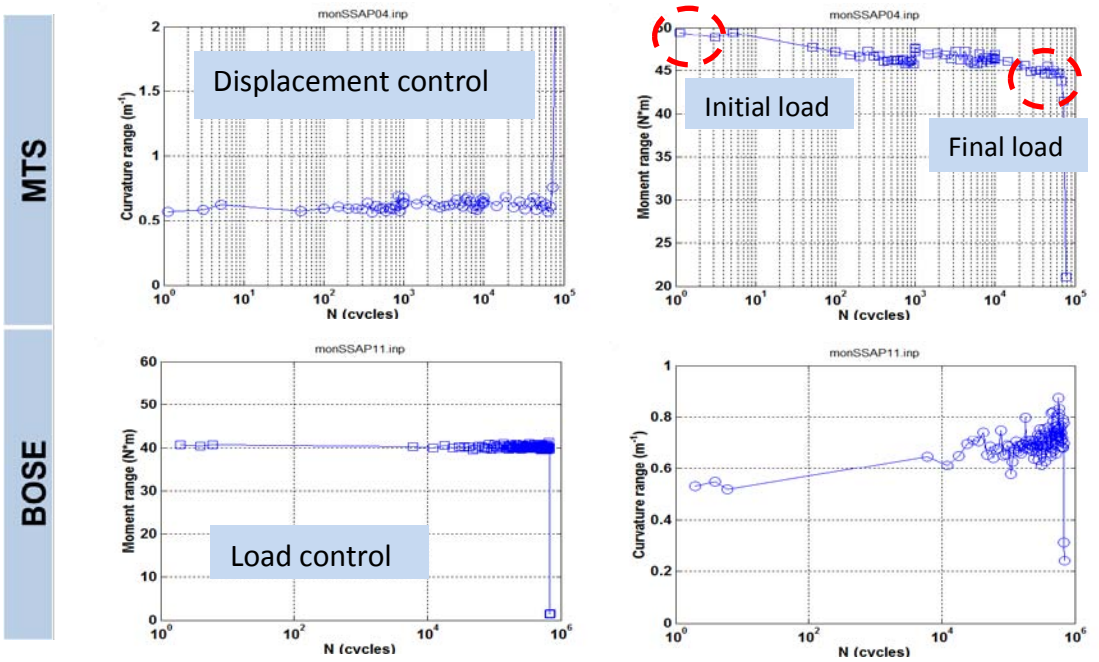

Fig. 20 The degraded surrogate rod due to cyclic loading reveals itself with a decrease in bending moment resistance from MTS displacement control mode data; while as in Bose load control mode data an increase in curvature was observed.

Fig. 21 shows the summary of the Bose and MTS bending fatigue data, where the load control Bose data is within the bonds between the initial load and final fracture load observed from the displacement control MTS data. The load specified in the vertical axis is referred to the force applied at the end of the rigid arms (4-in. long) of the U-bent tester to induce pure moment on the surrogate rods.

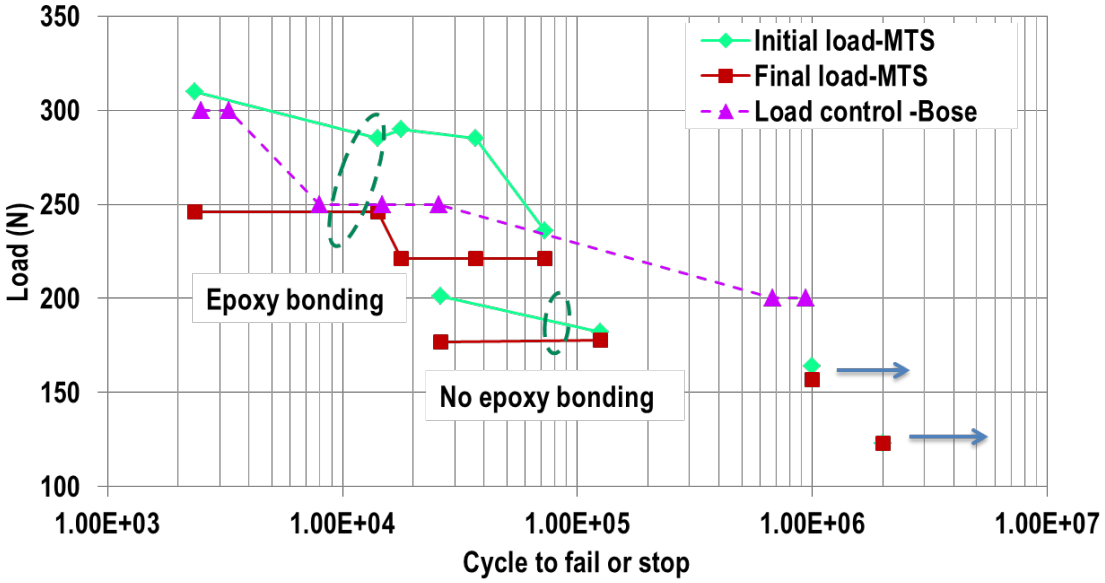

Fig. 21 Similar S-N curve trend was shown from displacement control data and load control data. The fatigue strength also appears to be dependent on interface bonding, SSAP samples w/o epoxy bond appears to have much lower fatigue endurance limit.

A SS tube with a single alumina rod insert (w/o epoxy bond) was also tested with reversal pure bending on a MTS machine with increased applied displacement at the rigid arms of the U-bent tester. The test results are shown in Fig. 22. In the low deflection region, the composite rod behaves like linear elastic material, and most of the load was carried by the alumina rod due to higher rigidity. While upon fracture of the inserted alumina rod, Fig. 22 shows a sudden load drop at 9-mm displacement cycle and an initiation of nonlinear (or yield) response with hysteresis loop formed accordingly. This indicates that composite rod load carrying capacity was suddenly transferred to the SS clad and results in localized yield of SS clad due to pellet-clad pinning, at region near the alumina rod fractured site. This observed composite rod load transferred mechanism may deserve our special attention; since it may imply to that the fuel integrity can have adverse impact to the fuel clad performance/integrity. Thus, a failed fuel pellet, such as crack or fracture, can certainly increase the inertia load carrying capacity to clad as well as to increase the probability of pellet-clad pinning interaction during transportation.

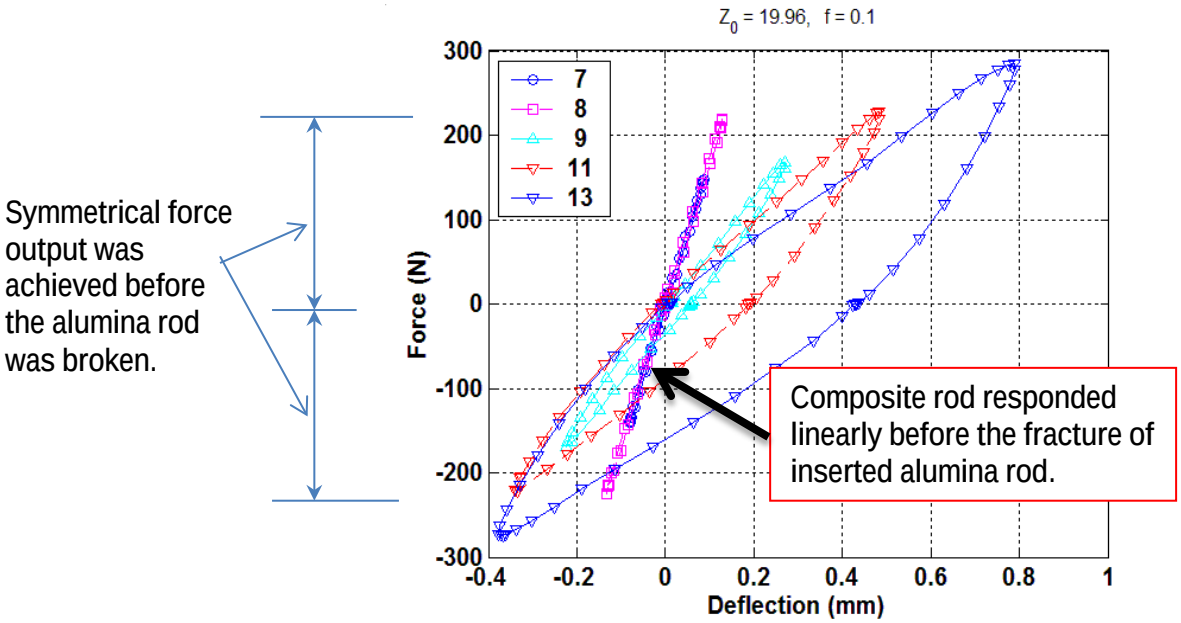

Fig. 22 Displacement control was used on MTS with amplitude 3-13-mm (as indicated in the legend) and the deflection was measured at mid-point of the rod. The composite rod bending test results indicate that before inserted alumina rod fracture, most of the bending load carrying capacity was resided on alumina rod. Upon alumina insert fractured, sudden load transfer will occur and SS tube starts to carry majority of bending moment; which results in plastic deformation of SS clad.

VIII. PRE-HYDRIDE ZR-4 SURROGATED ROD BENDING FATIGUE TESTING

The pre-hydride Zr-4 clad material was prepared with 500 ppm hydrogen content. The composite rod made of pre-hydride Zr-4 tube was filled with cast epoxy and used as a surrogate rod for the bending fatigue integrity study. The cast epoxy filled surrogate rod performs better than the SSAP sample due to a lack of pellet-clad pinning interaction. Some comparison results for the SS tube only and SSAP 02 (no epoxy bond), and composite rod of SS or pre-hydride Zr-4 tube filled with cast epoxy, are shown in Fig. 23 and Fig. 24, respectively. The SEM examination was also performed on the fractured ZrE01 pre-hydride sample, as shown in Fig. 25. The second pre-hydride surrogated rod ZrE02 was also under cyclic bending fatigue test, starting with lower displacement amplitudes of 4-mm and 6-mm. However, after 2.5M cycles no apparent degradation was observed so the test specimen was subjected to additional cycling with displacement amplitude of 8-mm. The ZrE02 finally failed at 1.9E+4 cycles with 5% reduction in flexural rigidity. The associated flexural rigidity and fracture images are shown in Fig. 26 and Fig. 27, respectively.

SS02, SS tube only	SSAP02, SS tube + 10 alumina segments
Cycling: ±4mm, 2Hz; Nf = 2.95E+04	Cycling: ±4mm, 2Hz; Nf = 2.62E+04

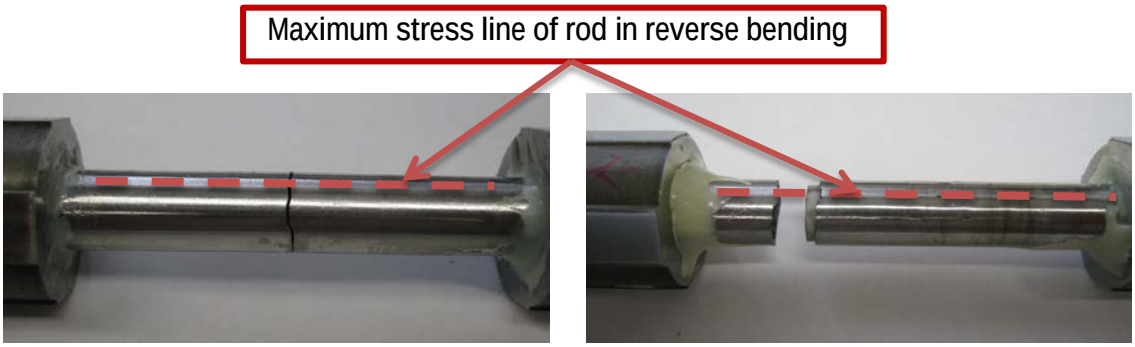

Fig. 23 Both tests are failed at gage section, done on a MTS machine. SSAP02 (w/o epoxy bond) failed earlier than tested sample of SS tube only.

SSE01, SS tube + cast epoxy	Hydrided Zry-4 tube + cast epoxy
Cycling: ±4mm, 2Hz; Nf = 5.45E+05	Cycling: ±8mm, 2Hz; Nf = 1.45E+04

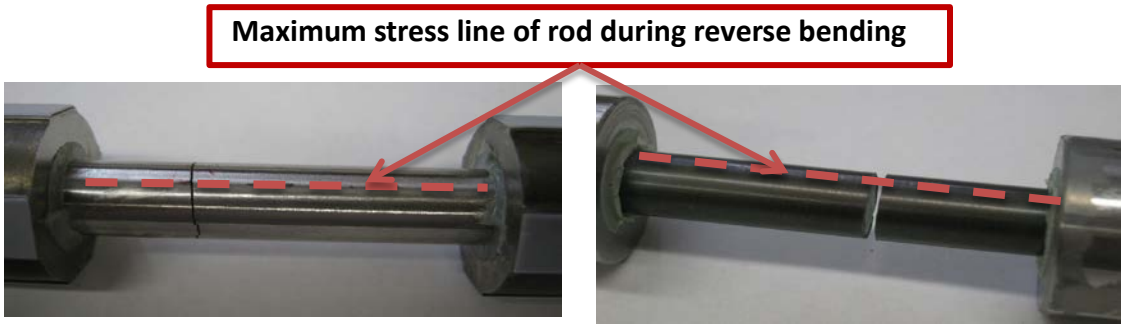

Fig. 24 SS tube with cast epoxy performed much better than that of S tube as well as SSAP02 surrogate rod. ZrE01 with filled cast epoxy also performed well.

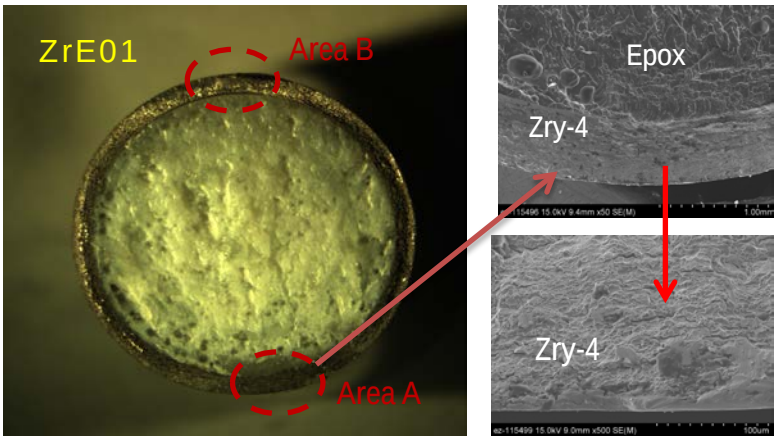

Fig. 25 Fracture Surface of Hydrided Zry-4 surrogate Rod, ZrE01. Fracture surface around area *A* (highest bending moment location) revealed striations resulting from cyclic crack propagation.

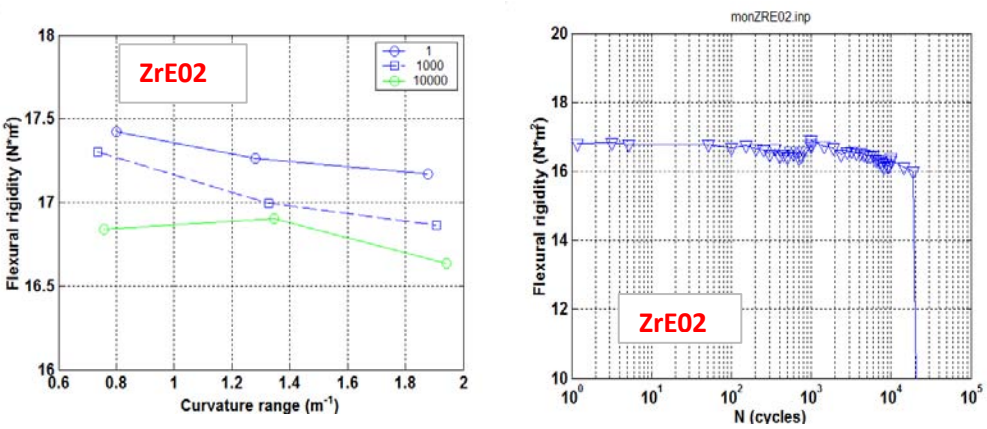

Fig. 26 Rod ZrE02 was made of pre-hydrided Zry-4 cladding + cast epoxy. Specimen had been cycled with amplitudes ±4 and ±6mm before applying 8-mm amplitude loading. Static measurements were conducted at three intervals, no significant degradation of flexural rigidity was observed. On-line monitoring demonstrated an equivalent decrease (5%) in flexural rigidity prior to rod failure.

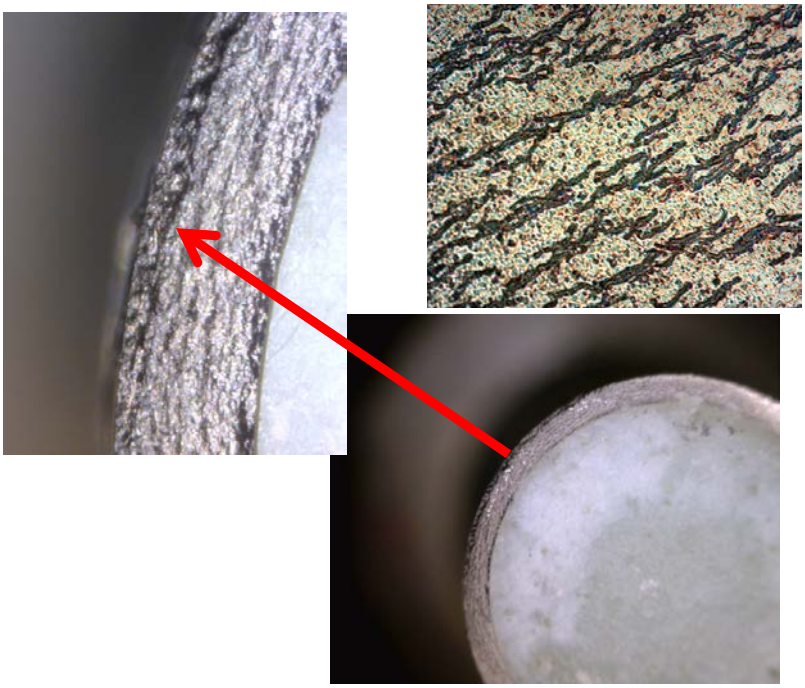

Fig. 27 Optical image of the cross section of tested pre-hydrided Zry-4 sample ZrE02. The delamination of Zr-4 and cast-epoxy at highest bending moment location was observed. The potential circumferential hydride delamination also indicated, shown to the left of Fig. 27, at the outer hydride ring region; the cyclic shear stress induced by the bending loading in the pre-hydride clad could be the root cause, in addition to the flexural normal stress fields. In reversal bending mode, the surrogate rod will experience both flexural normal tensile/compressive stress as well as more or less uniform shear stress across the cross-section of the rod system. The potential of such combined mixed-mode loadings induced mixed-modes failure to SNF vibration integrity deserves our special attention.

IX. FUTURE INITIATIVES ON SNF VIBRATION INTEGRITY STUDY

The developed reversal U-bent tester is currently under final stage of upgrading for hot-cell operation. The device is scheduled to be installed into the hot-cell during the summer of 2013 to start with reversal bending fatigue testing on the high burn-up SNF. Three proposed follow-on research topics regarding the continuing development of the SNF vibration integrity initiative are described below.

1. Developing semi-empirical characterization protocol for evaluating the fuel clad interaction and the impact of pellet-clad bonding to the effective lifetime of fuel-clad structure bending fatigue performance.
2. Collecting and evaluating the generated SNF vibration experimental data through statistical analyses tools to effectively understand the aging properties of clad, fuel and their cohesion bond, and the overall relation of clad-fuel structural response to individual component mechanical property evolutions.
3. Developing the accumulated damage index in assisting SNF effective lifetime evaluation under normal transportation vibration mode through using the target amplitude ranges and testing cycles based on transportation vibration time history data.

The developed reversal U-bent tester is designed to simulate the normal transportation related vibration, however, for periodic transient shocks experienced by rail or truck transportation and normal handling drop impact, a higher loading-rate device would be required. Thus, based on the developed U-bent concept, to build an integrated high loading-rate U-bent tester to simulate transient shock or handling-drop impact is also of interest.

Due to higher stiffness/rigidity (low fracture toughness and low ductility) of oxide fuel compared to that of Zr clad, the fused fuel pellets of high burn-up SNF will have a higher probability to fail or fracture than that of Zr clad under shock impact loading (i.e., the pellet damage loading threshold is lower than that of Zr-clad). Based on the surrogate data, it clearly indicates that due to higher stiffness of fuel pellet it can carry more moment resistance than clad if pellets and pellet-pellet/pellet-clad interface bonding remain intact. However, the oxide fracture toughness can degrade significantly under high-rate loading, if the fuel pellet fracture/debond threshold was reached under transient shock loading, the majority of moment resistance capacity will then shift to clad accordingly. This will result in an accelerated degradation of fuel clad under continuing vibration loading as demonstrated in Fig. 22. Thus, in order to have a more realistic and accurate SNF vibration reliability evaluation, the investigation on the impact of high rate loading, such as transient shock or handling drop loading, to the accumulated damage of SNF system under normal transportation will be essential.

X. CONCLUSIONS

The test system can be used to test and characterize static bending stiffness as well as the vibration integrity of spent nuclear fuel. The reversal bending is conducted utilizing a U-frame setup with the push-pull motion applied at the force loading point. The U-frame setup can be integrated into a test machine in either a vertical or horizontal position. The deformation of a rod specimen is measured using three-point deflection, and from that data, the curvature of a deformed rod specimen can be estimated.

A U-frame assisted bending fatigue test system has been proposed and developed in this study. Modifications and upgrades occurred during the process in order to obtain a reversal pure bending condition and at the same time, to make the setup friendly for hot-cell testing. The current version of the test system features a horizontal layout of the U-frame that is integrated in a Bose dual linear motor TestBench. The LRB sets are embedded in the rigid arms and pre-loaded to enable the reversal pure

bending of the U-frame without any concern over the backlash. The adapted horizontal layout also eliminates the effect of the weight of the U-frame components on the deformation of the rod specimen that would exist should a vertical layout setup be used. In addition, loads on both sides of the U-frame enabled by Bose dual linear motors are critical to deliver a symmetrical loading to the setup in a dynamic loading condition. The single-side loading can create serious concern over the stress state applied to the rod specimen because the time is required for stress waves to propagate from the loading end to the un-loading end of the rod specimen. Moreover, the electromagnetic force-based test system is found to be more reliable and compact than a conventional servo-hydraulic system.

The three-point deflection measurement implemented in this study focuses on the deformation of the rod specimen instead of the total deformation that would occur in a single-point deflection measurement. The curvature of the deformed rod specimen can be calculated and the flexural rigidity can be defined readily. The flexural rigidity could depend on the level of curvature applied. However, this doesn't prevent it from characterizing the property of the rod specimen in a cycle test. In the cyclic fatigue test, the variation of flexural rigidity under a defined moment or curvature is the focus of the data collection, and the variation with increased cycles indicates the degradation of rod property.

The relationship of total strain or bending moment versus the number of cycles to failure exhibits a defined trend. Under a displacement or load control mode, it is observed that the lifetime of the rod in the cycle tests decreased with the increase in the total strain or load applied. It is also revealed that the clad-pellet bonding may play a certain role in the fatigue of the rod. This finding suggests an important effect of the cladding-pellet interaction on the fatigue response of spent fuel and remains to be investigated.

ACKNOWLEDGMENTS

Authors would like thank Ting Tan, Hao Jiang, Thomas Cox, Chuck Baldwin, and Yong Yan for their supports, and John Scaglione and Edgar Lara-Curzio for reviewing this paper. Authors also want to thank Gordon Bjorkman and Bob Einziger for providing valuable comments during the program development. The project is sponsored by Nuclear Regulatory Research, U.S. Nuclear Regulatory Commission under DOE contract DE-AC05-00OR22725 with UT-Battelle, LLC.

REFERENCES

1. Wang, J.-A. J., Wang, H., Yan, Y., Howard, R., and Bevard, B., High burn-up spent fuel vibration integrity study progress letter report (out-of-cell fatigue testing development – Task 2.1), ORNL/ TM-2010/288, Jan 2011
2. Wang, J.-A. J., Wang, H., Tan, T., Jiang, H., Cox, T., Yan, Y., Progress letter report on U-frame test setup and bending fatigue test for vibration integrity study (out-of-cell fatigue testing development – Task 2.2), ORNL/TM- 2011/531, January, 2012.
3. Wang, J.-A. J., Wang, H., Cox, T., Yan, Y., Progress letter report on U-frame test setup and bending fatigue test for vibration integrity study (out-of-cell fatigue testing development – Task 2.3), ORNL/TM-2012/417, August, 2012.
4. Hong Wang, Jy-An John Wang, Ting Tan, Hao Jiang, Thomas S. Cox, Rob L. Howard, Bruce B. Bevard, and Michelle Flanagan, "Development of U-frame bending system for studying the vibration integrity of spent nuclear fuel," *Journal of Nuclear Materials*, 440 (2013) 201-213.